Invited Paper

Optical signal processing using silicon resonance and slow-light structures

Linjie Zhou, Jianping Chen, Xiaomeng Sun, Jingya Xie, and Haike Zhu
State Key Laboratory of Advanced Optical Communication Systems and Networks
Department of Electronic Engineering, Shanghai Jiao Tong University, Shanghai 200240, China

Email: ljzhou@sjtu.edu.cn

ABSTRACT

We present our recent work on silicon resonance and slow-light based devices for optical signal processing. Waveguide self-coupling and mutual coupling are used to tailor the waveguide spectral and dispersion characteristics. With self-coupling, optical resonances are generated with unique transmission performances. Electromagnetically induced transparency (EIT)-like effect appears in cascaded self-coupled waveguides. With mutual coupling between ridge and slot waveguides, group velocity experiences a big jump and optical signal can be delayed for a large range with low distortion by using thermo-optic tuning.

Keywords: silicon photonics, waveguides, microresonators, optical delay, optical signal processing, electromagnetically induced transparency, slot waveguides

1. INTRODUCTION

Silicon photonic devices have attracted a lot of research interests in recent years and multiple basic passive and active optical components have been demonstrated including waveguides [1-3], filters [4, 5], switches [6, 7], modulators [8, 9], detectors [10, 11], and lasers [12, 13]. These individual components or their combinations can be employed for various kinds of on-chip optical signal processing. In particular, silicon–organic hybrid slot waveguides, possessing the merits of high confinement of silicon waveguide and high nonlinear effect of electro-optic polymer, can be used for all-optical high-speed signal processing [1, 14]. Slow light structures can also be used to enhance the interaction between light and silicon material to amplify nonlinear effects since light intensity is greatly enhanced due to the reduced group velocity. Silicon microring resonators and photonic crystal waveguides are the most widely adopted slow light structures [15, 16]. On-chip integrated optical systems such as transceivers, comprising modulators, detectors, multiplexing/demultiplexing components, and electronic driving circuits, have also been demonstrated [17, 18].

Here we present waveguide-coupling based silicon photonic devices for optical signal filtering and buffering. Wavelength division multiplexing (WDM) filters are a basic element in frequency-domain optical signal processing. WDM filters can be made using interference or resonance structures. Microresonator-based WDM filters are very attractive as they have a small footprint and their central wavelength and spectral line-shape can be easily reconfigured [19, 20]. On the other side, optical signal buffering is a fundamental function in time-domain optical signal processing. As photons cannot be stored, current buffering methods mostly rely on slow-light to delay optical signals [21, 22]. The filtering and buffering functionalities are implemented though tailoring the dispersion of the corresponding waveguides or devices. Waveguide coupling is an effect way to alter waveguide transmission and dispersion performances. We present two types of structures to make use of waveguide coupling to tailor the spectral and temporal properties. In one configuration, coupling is enabled by a single bent waveguide, which produces interfered resonances. In the second configuration, coupling is imposed between a ridge waveguide and a slot waveguide, which induces strong dispersion near the wavelength where phase matching condition is satisfied.

Silicon Photonics VII, edited by Joel Kubby, Graham Trevor Reed, Proc. of SPIE Vol. 8266,
82660N · © 2012 SPIE · CCC code: 0277-786X/12/$18 · doi: 10.1117/12.908194

2. SELF-COUPLED OPTICAL WAVEGUIDE

Self-coupled optical waveguides (SCOWs) are novel resonance devices, formed by a single bent waveguide [23, 24]. Light circulates inside the self-coupled waveguide to form optical resonances. For the simplest form of SCOW resonators [24], the clockwise (CW) and counter-clockwise (CCW) resonance modes are co-excited and they are connected through the central bridge waveguide. Most notably, these degenerate resonance modes are not mutually coupled but sequentially excited, i.e., energy transfer is unidirectional from one mode to the other. This unique feature makes them quite different from conventional microring resonators, and hence exhibiting distinct transmission behaviors. Previously, we investigated their performances when the couplers are symmetric, and in the following we focus on SCOW resonators with asymmetric coupling.

2.1 Single-stage SCOW resonator

We first analyze a single-stage SCOW resonator as shown schematically in Fig. 1 (a). There are two couplers in the structure with coupling coefficients of κ_1 and κ_2. The SCOW resonator transmission performance is quite dependent on these coupling coefficients. In practice, these two coupling coefficients can be obtained by using directional couplers with different lengths or gap separations.

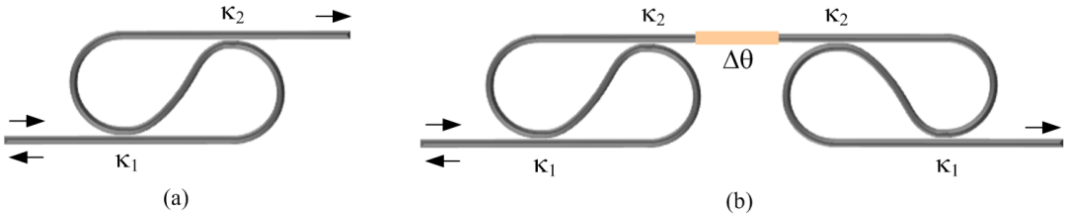

Figure 1. Schematic illustrations of (a) single-stage and (b) double-stage SCOW resonances.

Figure 2 (a) shows the transmission (T) and reflection (R) spectra for a single-stage SCOW resonator when light is coupled from the left- and right-ends. The coupling coefficients are $\kappa_1 = 0.74$ and $\kappa_2 = 0.95$, which means that light is more easily coupled to the resonator from the left-end. The resonator loss factor is assumed to be 0.999, corresponding to ~2 dB/cm waveguide propagation loss for a 50 μm resonance round-trip. The transmission spectra are exactly overlapped, which is expected since it is a reciprocal system. Interestingly, the reflection spectra show different peak intensities, with the right-end reflection incurring more loss. The reflection resonance peak is flat, which is desirable for optical filter applications, where multiple wavelength channels can be simultaneously extracted. Figure 2 (b) shows the transmission and reflection phase responses for the SCOW resonator. The phase changes rapidly around the resonance wavelength. It should be noted that phase swing of the left-end reflection is three times larger than that of the right-end reflection. As group delay is the first-order derivative of phase to frequency, the large phase swing leads to a high group delay as shown in Fig. 2 (c). Given that the group delay from the left and right ends have the same bandwidth, the left-end reflection has a delay-bandwidth product three times higher than that of the right-end. In comparison, a micoring all-pass filter working at over-coupling regime has a phase swing in between. Therefore, the left-end reflection is more efficient in terms of optical signal buffering. However, it also has high group delay dispersion around resonance, which can cause distortion to the delayed signal. The right-end reflection instead has a lower but flatter group delay, together with a lower insertion loss over a broad spectral range.

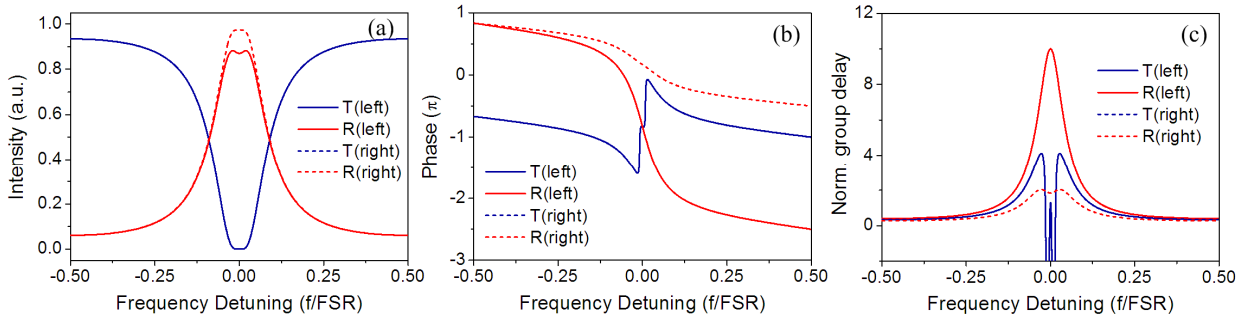

Figure 2. Optical responses of a SCOW resonator. The coupling coefficients are $\kappa_1 = 0.74$ and $\kappa_2 = 0.95$. (a) is the optical intensity response, (b) is the phase response, and (c) is the group delay response. Group delay is normalized to the resonator round-trip group delay. Frequency detuning is normalized to the free spectral range (FSR) of the SCOW resonator.

2.2 Double-stage SCOW resonators

The optical responses for cascaded SCOW resonators are more complicated, as another set of resonances will be generated between adjacent SCOW resonators due to resonant feedback. Here we only consider double-stage SCOW resonators with each having asymmetric coupling coefficients. Figure 3 (a) and (b) show the transmission and reflection spectra when the large group delay end is positioned inside to form inter-SCOW resonances. As the reflection from a SCOW resonator experiences a large group delay, the inter-SCOW resonances can be regarded as formed by slow-light. Therefore, inside the high reflection band, sharp EIT-like peaks and dips appear. In Fig. 3 (a), there are essentially three EIT-like resonances with the central one highly suppressed due to waveguide loss. Figure 3 (b) shows the shift of EIT-like resonances when a $\pi/2$ phase shift is introduced to the connection waveguide between the SCOW resonators. Two sharp resonances are clearly observed in a broad high reflection band. Figure 3 (c) and (d) show the transmission and reflection spectra when the small group delay end of the SCOW resonator is positioned inside. In this case, the number of EIT-like resonances is reduced because the reflection phase swing is smaller compared to the previous case. In order to more clearly show the EIT-like peaks, we also plot several transmission spectra with various coupling coefficients in Fig. 4. The resonator loss factor is set at $a = 0.9999$ (~0.2 dB/cm waveguide loss). With a reduction in the coupling coefficient κ_1, the SCOW resonator reflectivity reduces, and hence light is more easily tunneling through the two SCOW resonators, making the EIT-like resonance peak higher and broader.

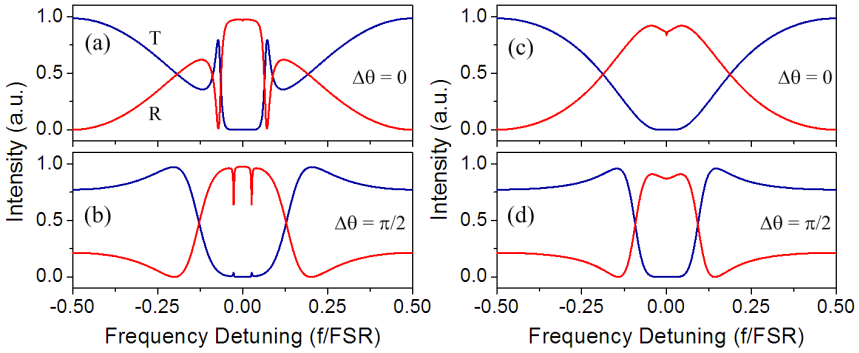

Figure 3. Optical transmission and reflection spectra of two-stage SCOW resonators. The coupling coefficients are $\kappa_1 = 0.95$ and $\kappa_2 = 0.74$ for (a) and (b), and $\kappa_1 = 0.74$ and $\kappa_2 = 0.95$ for (c) and (d). In (a) and (c) the inter-SCOW resonance is coincident with the SCOW resonance, and in (b) and (d) they are totally out of phase. The inter-SCOW resonance is assumed to have a free spectral range (FSR) equal to that of the SCOW resonator. The SCOW resonator loss factor is $a = 0.999$.

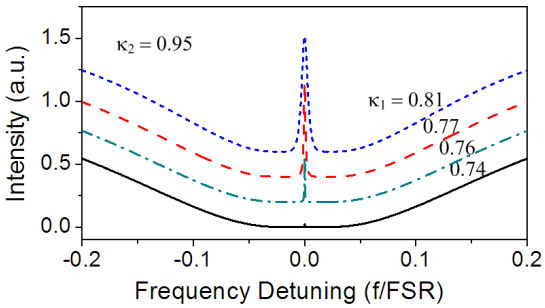

Figure 4. EIT-like resonance spectra in two-stage SCOW resonators. SCOW resonator loss factor is $a = 0.9999$.

The EIT-like resonances, featured with sharp and narrow resonance peaks, can be employed for many optical signal processing applications, such as ultra-narrow band optical filtering, optical signal buffering, and high-resolution

nonlinear signal processing etc. The cascaded SCOW resonators presented here open a new way to conveniently generate on-chip analog of EIT.

3. COUPLED-MODE COMPOSITE OPTICAL WAVEGUIDE

Waveguide mutual coupling is an effective way to tailor the dispersion characteristics [25, 26]. From the coupled mode theory, there exist two complimentary supermodes with symmetric and asymmetric electric-field profiles in coupled waveguides. These supermodes are highly dispersive around the crossing-point. For the symmetric supermode, optical power is more concentrated in the waveguide with a higher effective refractive index, and it is opposite for the asymmetric supermode. Therefore, across the crossing-point there is an energy shift from one waveguide to the other. If the coupled waveguides are made from slow and fast light, then the group velocity undergoes a big jump across the coupling point. Based on this, we design a composite waveguide composed by a regular ridge waveguide and a slot waveguide to function as a tunable delay line for optical signals.

3.1 Transmission characteristics

Figure 5 (a) shows the schematic of the coupled-mode composite optical waveguide. The ridge and slot waveguides support their own guided modes with distinct mode profiles. Optical power is mainly confined in the waveguide core for the ridge waveguide. In contrast, a substantial part of the optical power is confined in the nano-slot for the slot waveguide due to the discontinuity of electric-field across the interfaces (for the quasi-TE polarization). This leads to distinct dispersion behaviors for these waveguides. The dashed lines in Fig. 5 (b) show the waveguide effective refractive index dispersion. The ridge waveguide has large waveguide dispersion and the group refractive index is close to 5.5 for a 300 nm×340 nm ridge waveguide. The slot waveguide has more energy confined in the air slot and the group index is 3.6 for a 440 nm×340 nm slot waveguide with a 20 nm slot in center. The supermodes for the composite waveguide have their dispersion curves bent near the crossing point, as shown by the solid curves in Fig. 5 (a). The anti-crossing of the supermode dispersion curves indicates that, the symmetric supermode is closer to the ridge waveguide mode at the shorter wavelength side, and closer to the slot waveguide mode at the longer wavelength side, as shown in Fig. 5 (e)-(f). Therefore, its group velocity experiences a rapid increase around the anti-crossing wavelength. The asymmetric supermode has an opposite effect with its group velocity drops near the anti-crossing wavelength. The solid curves in Fig. 5 (c) show the group refractive indices for the symmetric and asymmetric supermodes.

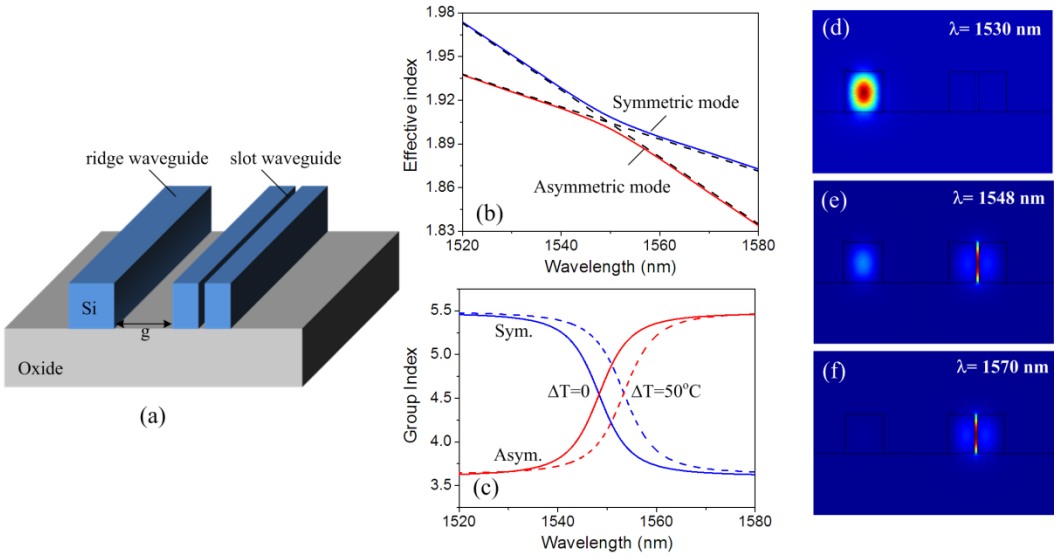

Figure 5. (a) Schematic of a coupled-mode composite optical waveguide. (b) Effective refractive index dispersion diagram. (c) Group refractive index dispersion diagram. (d)-(f) Symmetric supermode power profiles at three wavelengths. The ridge waveguide dimension is 300 nm (W) × 340 nm (H), and the slot waveguide dimension is 440 nm (W) × 340 nm (H) with a 20 nm slot in the center. The separation between these two waveguide is 500 nm. Silicon and oxide refractive indices are chosen to be 3.478 and 1.444, respectively.

The coupling strength between the ridge and slot waveguides plays an important role in the supermode dispersion. With an increase in the coupling strength, the anti-crossing spectral window becomes broader. Figure 6 (a) shows the group index dispersion curves for various gap sizes. The group index transition occurs over a narrow range for a large gap size.

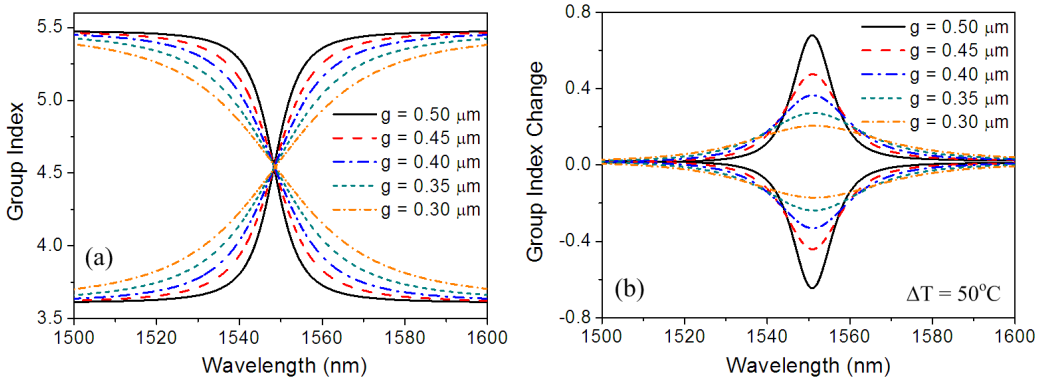

Figure 6. (a) Group index dispersion curves for various gap sizes. (b) Group index change for a temperature increment of 50°C.

Because of their distinct mode profiles, the supermodes have different temperature dependence. When the temperature rises, the refractive indices of the silicon and oxide materials both increase with thermo-optic coefficients of 1.86×10^{-4} and 9.34×10^{-6}, respectively. Hence, the dispersion curves of the ridge and slot waveguides in Fig. 5 (b) both move upward. As the slot waveguide is less sensitive to temperature variation, the crossing point eventually moves towards the longer wavelength side. As a result, the group index increases for the symmetric supermode and decreases for the asymmetric supermode. Figure 6 (b) shows the group index change for various gap sizes when the temperate increases for 50°C. It shows that the group index change has a strong dependence on wavelength and reaches the maximum at the crossing point, which implies that the waveguide mutual coupling can amplify the group index sensitivity to temperature. The amplification factor is dependent on the coupling strength. The weaker the coupling is, the more the sensitivity is amplified. It should be noted that the coupling cannot be very weak in practice, because in that case the effective indices of the two supermodes are very close to each other and a small structural variation can excite the other supermode.

The high temperature sensitivity of the group index near the crossing point means that a signal can be delayed for a relatively large range by tuning the temperature. If the signal is carried by the symmetric supermode, its delay increases when temperature rises. Instead, if it is carried by the asymmetric supermode, its delay reduces with temperature. From Fig. 6 (b), it can also be seen that the group index change becomes sharper and narrower for weaker coupling, which implies that a larger delay change is always obtained at the expense of a smaller bandwidth for a certain waveguide length. In other words, its delay performance is limited by the delay-bandwidth product constraint, similar to other slow light systems, e.g., microring resonators.

Although the group delay is very sensitive to temperature variation near the crossing point, the corresponding group delay dispersion is also very large. Figure 7 (a) shows the abnormal group delay dispersion of the symmetric supermode in a 10-cm long composite waveguide. If a narrow optical pulse is transmitted upon this supermode, it will be gradually broadened by the group delay dispersion. Figure 7 (b) shows the transmitted pulses with and without temperature tuning, together with the initial input pulse. The input pulse has a Gaussian shape with a half width of 10 ps, and its carrier wavelength is at the crossing point. A temperature increment of 50 °C induces ~190 ps delay to the transmitted pulse. It is interesting to note that pulse distortion is reduced when the temperature rises because of the red-shift of the dispersion curve. Figure 7 (c) and (d) show the dispersion curve and the corresponding delay when the optical pulse is carried by the asymmetric mode. In this case, when the temperature rises, the pulse is less delayed with a reduced distortion. Comparing Fig. 7 (a) and (c), we notice that the dispersion curves for the symmetric and asymmetric supermodes are complimentary, and hence the dispersion can be compensated by cascading two segments of composite waveguides with opposite supermodes. Figure 7 (e) shows the total dispersion for such a composite waveguide composed by two 5-cm long waveguide segments for each to excite one supermode. The dispersion is almost flat and the transmitted pulse is almost identical to the initial one after propagation as shown in Fig. 7 (f). The pulse can be relatively delayed or advanced by heating up one of the waveguide segments. Once one of the dispersion curves shifts, the total dispersion is

no longer in exact compensation, resulting in a little dispersion to the transmitted pulse. The delay tuning range for a temperature increment of 50°C is ~190 ps, close to those in the previous two cases. However, its dispersion is greatly reduced facilitating high speed optical signal transmission.

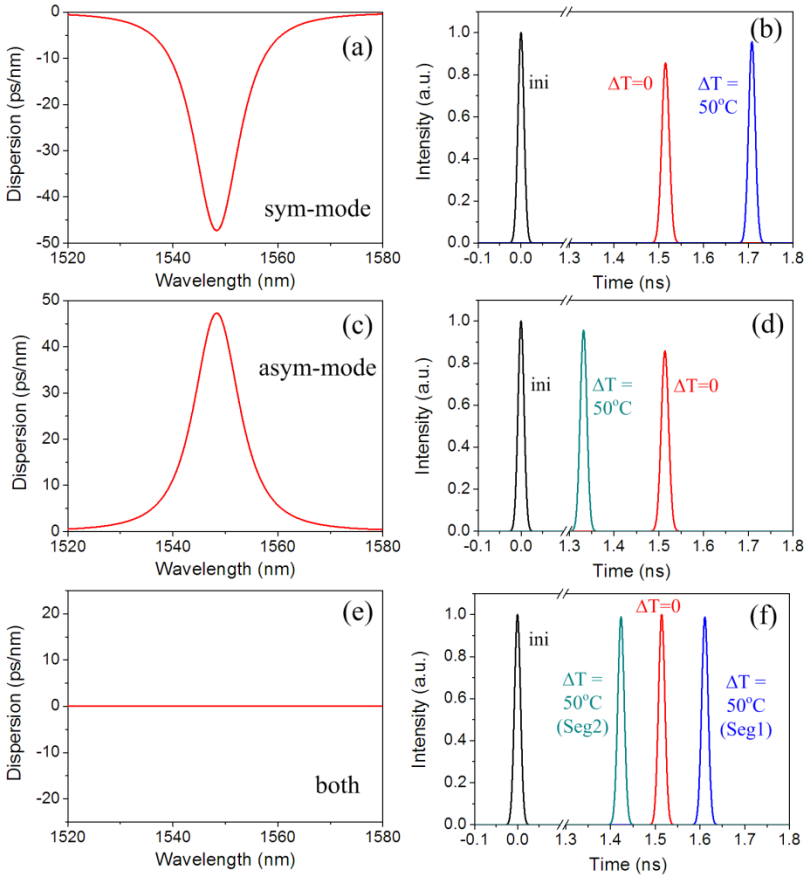

Figure 7. Group velocity dispersion and pulse propagation in 10-cm long coupled-mode composite optical waveguides. In (a) and (b), optical signal is carried by the symmetric supermode; in (c) and (d), optical signal is carried by the asymmetric supermode; in (e) and (f), half of the waveguide is excited with the symmetric mode and half is excited with the asymmetric mode.

3.2 Mode conversion

As seen from previous discussions, there always exist two complementary supermodes in the composite waveguide. The key to obtain a controllable signal delay is to properly excite one supermode. We use a mode converter to gradually transform the supermode to the ridge or slot waveguide mode. When the ridge waveguide is gradually widened, its mode effective index increases, resulting in an up-shift of its dispersion curve. The anti-crossing point moves to the longer wavelength side, and thus the symmetric supermode is more close to the ridge waveguide mode. In this way, the symmetric supermode is gradually transformed to the ridge waveguide mode. Figure 8 (a) shows schematically the mode converter structure and (b) shows the BPM simulated optical power flow in the mode converter when the symmetric supermode is excited at the input. It should be noted that in order not to excite the asymmetric supermode in the composite waveguide, the ridge waveguide should be adiabatically tapered where optical power couples unidirectionally to the slot waveguide, or otherwise it will induce an optical power oscillation. On the other hand, if the asymmetric supermode is input to the converter, then it is gradually transformed to the slot waveguide mode, as shown in Fig. 8 (c). Figure 8 (d)-(f) show the mode conversion when the ridge waveguide is gradually narrowed. In this case, the conversion is just reversed, i.e., the symmetric mode is transformed to the slot waveguide mode and the asymmetric mode is transformed to the ridge waveguide mode. Therefore, the supermodes in the composite waveguide can be selectively

excited by tapering the ridge waveguide, and the transition between these two supermodes can be realized with the aid of a single tapered ridge waveguide.

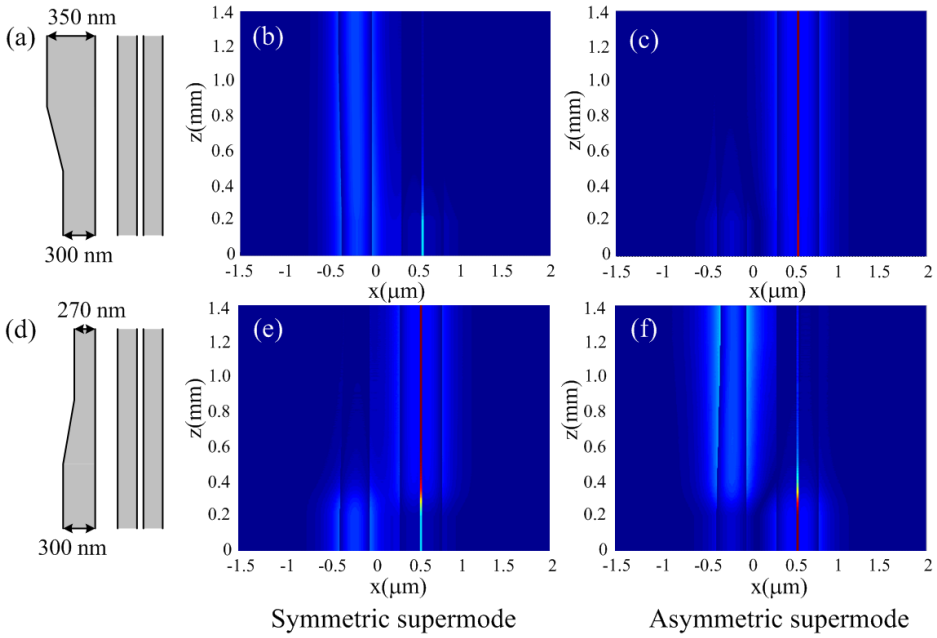

Figure 8. 2D BPM simulations of mode converters. In (a)-(c) the ridge waveguide is adiabatically tapered up, and in (d)-(f) the ridge waveguide is adiabatically tapered down. The waveguide refractive index is chosen to be 2.11 and cladding refractive index 1 to take into account the vertical confinement. The gap size is 0.3 μm.

4. CONCLUSIONS

In summary, we presented two types of waveguide-coupling based passive devices for optical signal processing. The optical transmission and dispersion responses are tailored by waveguide self-coupling and mutual-coupling. Due to waveguide self-coupling, light circulates bi-directionally inside the SCOW resonator, resulting in optical resonances. The cascaded SCOW resonators exhibit an electromagnetically induced transparency (EIT)-like resonances, manifested as sharp peaks appearing in an opaque spectral window. For the coupled-mode composite waveguide, its waveguide dispersion is quite dependent on the coupling between the ridge waveguide and the slot waveguide. Using thermal tuning, the optical signal delay in the composite waveguide can be varied for a large range. The group velocity dispersion can be compensated by cascading two segments of composite waveguides with opposite mode polarities. These waveguide-coupling based passive devices have potential applications in frequency-domain and time-domain optical signal processing.

5. ACKNOWLEDGEMENTS

This work was supported in part by the 973 Program (2011CB301700), the National Natural Science Foundation of China (NSFC) (61007039 and 61001074), the Science and Technology Commission of Shanghai Municipality (STCSM) Project (10DJ1400402), and the State Key Lab Projects (GKZD030020).

REFERENCES

[1] J. Leuthold, W. Freude, J. M. Brosi *et al.*, "Silicon organic hybrid technology—A platform for practical nonlinear optics," Proceedings of the IEEE, 97(7), 1304-1316 (2009).

[2] C. Koos, L. Jacome, C. Poulton *et al.*, "Nonlinear silicon-on-insulator waveguides for all-optical signal processing," Optics Express, 15(10), 5976-5990 (2007).

[3] X. Liu, R. M. Osgood, Y. A. Vlasov *et al.*, "Mid-infrared optical parametric amplifier using silicon nanophotonic waveguides," Nature Photonics, 4(8), 557-560 (2010).

[4] L. Zhou, and A. W. Poon, "Electrically reconfigurable silicon microring resonator-based filter with waveguide-coupled feedback," Optics Express, 15(15), 9194-9204 (2007).

[5] L. Zhou, and A. W. Poon, "Fano resonance-based electrically reconfigurable add-drop filters in silicon microring resonator-coupled Mach-Zehnder interferometers," Optics letters, 32(7), 781-783 (2007).

[6] T. Chu, H. Yamada, S. Ishida *et al.*, "Compact 1× N thermo-optic switches based on silicon photonic wire waveguides," Optics Express, 13(25), 10109-10114 (2005).

[7] M. W. Pruessner, T. H. Stievater, M. S. Ferraro *et al.*, "Thermo-optic tuning and switching in SOI waveguide Fabry-Perot microcavities," Optics Express, 15(12), 7557-7563 (2007).

[8] L. Zhou, and A. W. Poon, "Silicon electro-optic modulators using pin diodes embedded 10-micron-diameter microdisk resonators," Optics Express, 14(15), 6851-6857 (2006).

[9] T. Y. Liow, K. W. Ang, Q. Fang *et al.*, "Silicon modulators and germanium photodetectors on SOI: Monolithic integration, compatibility, and performance optimization," IEEE Journal of Selected Topics in Quantum Electronics , 16(1), 307-315 (2010).

[10] S. Liao, N. N. Feng, D. Feng *et al.*, "36 GHz submicron silicon waveguide germanium photodetector," Optics Express, 19(11), 10967-10972 (2011).

[11] L. Vivien, J. Osmond, J. M. Fédéli *et al.*, "42 GHz pin Germanium photodetector integrated in a silicon-on-insulator waveguide," Optics Express, 17(8), 6252-6257 (2009).

[12] A. W. Fang, H. Park, O. Cohen *et al.*, "Electrically pumped hybrid AlGaInAs-silicon evanescent laser," Opt. Express, 14(20), 9203-9210 (2006).

[13] D. Liang, M. Fiorentino, T. Okumura *et al.*, "Electrically-pumped compact hybrid silicon microring lasers for optical interconnects," Optics Express, 17(22), 20355-20364 (2009).

[14] C. Koos, P. Vorreau, T. Vallaitis *et al.*, "All-optical high-speed signal processing with silicon–organic hybrid slot waveguides," Nature Photonics, 3(4), 216-219 (2009).

[15] B. Corcoran, C. Monat, M. Pelusi *et al.*, "Optical signal processing on a silicon chip at 640Gb/s using slow-light," Optics Express, 18(8), 7770-7781 (2010).

[16] Y. A. Vlasov, M. O'Boyle, H. F. Hamann *et al.*, "Active control of slow light on a chip with photonic crystal waveguides," Nature, 438(7064), 65-69 (2005).

[17] C. Gunn, A. Narasimha, B. Analui *et al.*, "A 40Gbps CMOS photonics transceiver." Proc. SPIE 6477, 64770N (2007).

[18] A. Narasimha, B. Analui, Y. Liang *et al.*, "A Fully Integrated 4× 10-Gb/s DWDM Optoelectronic Transceiver Implemented in a Standard 0.13 μm CMOS SOI Technology," IEEE Journal of Solid-State Circuits, 42(12), 2736-2744 (2007).

[19] I. Kiyat, A. Aydinli, and N. Dagli, "Low-power thermooptical tuning of SOI resonator switch," IEEE Photonics Technology Letters , 18(2), 364-366 (2006).

[20] L. Zhou, S. S. Djordjevic, N. K. Fontaine *et al.*, "Silicon microring resonator-based reconfigurable optical lattice filter for on-chip optical signal processing." IEEE LEOS, 501-502 (2009).

[21] F. Xia, L. Sekaric, and Y. Vlasov, "Ultracompact optical buffers on a silicon chip," Nature Photonics, 1(1), 65-71 (2006).

[22] J. Adachi, N. Ishikura, H. Sasaki *et al.*, "Wide range tuning of slow light pulse in SOI photonic crystal coupled waveguide via folded chirping," IEEE Journal of Selected Topics in Quantum Electronics, 16(1), 192-199 (2010).

[23] L. Zhou, T. Ye, and J. Chen, "Waveguide self-coupling based reconfigurable resonance structure for optical filtering and delay," Optics Express, 19(9), 8032-8044 (2011).

[24] L. Zhou, T. Ye, and J. Chen, "Coherent interference induced transparency in self-coupled optical waveguide-based resonators," Optics letters, 36(1), 13-15 (2011).

[25] L. Zhang, Y. Yue, Y. Xiao-Li *et al.*, "Highly dispersive slot waveguides," Optics Express, 17(9), 7095-7101 (2009).

[26] U. Peschel, T. Peschel, and F. Lederer, "A compact device for highly efficient dispersion compensation in fiber transmission," Applied Physics Letters, 67, 2111 (1995).